

# CHARACTERISTICS AND FREQUENCY OF LARGE SUBMARINE LANDSLIDES AT THE WESTERN TIP OF THE GULF OF CORINTH

Arnaud Beckers<sup>1,2\*</sup>, Aurelia Hubert-Ferrari<sup>1</sup>, Christian Beck<sup>2</sup>, George Papatheodorou<sup>3</sup>, Marc de Batist<sup>4</sup>, Dimitris Sakellariou<sup>5</sup>, Efthymios Tripsanas<sup>6</sup>, Alain Demoulin<sup>1</sup>

<sup>1</sup> Department of Geography, University of Liège, allée du 6 août 2, 4000 Liège, Belgium. Email : beckersarnaud@gmail.com.

<sup>2</sup> ISTERre, CNRS UMR 5275, University of Savoie, F-73376 Le Bourget du Lac, France.

<sup>3</sup> Department of Geology, University of Patras, Greece

<sup>4</sup> Department of Geology and Soil Science, Gent

<sup>5</sup> Institute of Oceanography, Hellenic Center for Marine Research, GR-19013 Anavyssos, Greece

<sup>6</sup> Gnosis Geosciences, Edinburgh, EH10 5JN, U.K.

\* Now at: CSD Engineers, Namur Office Park 2, Avenue des dessus de Lives, 5101 Namur, Belgium

Correspondence to: Aurelia Hubert-Ferrari (aurelia.ferrari@ulg.ac.be)

## Abstract

Coastal and submarine landslides are frequent at the western tip of the Gulf of Corinth, where small to medium failure events ( $10^6$ - $10^7$  m<sup>3</sup>) occur on average every 30-50 years. These landslides trigger tsunamis, and consequently represent a significant hazard. We use here a dense grid of high-resolution seismic profiles to realize an inventory of the large mass transport deposits (MTDs) that result from these submarine landslides. Six large mass wasting events are identified, and their associated deposits locally represent 30% of the sedimentation since 130ka in the main western Basin. In the case of a large MTD of  $\sim 1$  km<sup>3</sup> volume, the simultaneous occurrence of different slope failures is inferred and suggests an earthquake triggering. However, the overall temporal distribution of MTDs would result from the time-dependent evolution of pre-conditioning factors, rather than from the recurrence of external triggers. Two likely main pre-conditioning factors are (1) the reloading time of slopes, which varied with the sedimentation rate, and (2) dramatic changes in water depth and water circulation that occurred 10-12ka ago during the last post-glacial transgression. Such sliding events likely generated large tsunami waves in the whole Gulf of Corinth, possibly larger than those reported in historical sources considering the observed volume of the MTDs.

## 1 Introduction

The study of marine geohazards through their imprint in the late Quaternary sedimentary record is of great significance, since it can provide further information on geohazard events recorded in historical records, or even extend this record to much earlier times. The identification and recurrence patterns of mass transport deposits (MTDs) resulting from submarine landslides in sedimentary basins and lakes provide valuable information on possibly associated tsunamis as well as their potential trigger (e.g. earthquake). Tsunami hazard is particularly an issue of concern in the Mediterranean Sea where more than 300 tsunamis have been listed in the historical and sedimentary records (Soloviev, 1990; Salamon et al., 2007; Lorito et al., 2008).

This paper focuses on the Gulf of Corinth, Greece, located in the most seismically active part of the Corinth Rift. This area shows one of the largest seismic hazard in Europe (Woessner et al., 2013) and is affected by a tsunami once every 19 years on average, leading to a significant risk (Papadopoulos, 2003; Papatheodorou and Dominey-Howes, 2003). The gulf's western tip is the most active part of the Corinth rift, characterized by an extension of  $15 \text{ mm.yr}^{-1}$  (Briole et al., 2000), and by frequent submarine or coastal landslides (e.g. Henzen et al., 1966; Papatheodorou and Ferentinos, 1997; Lykousis et al., 2009). Small to medium failure events ( $10^6$ - $10^7$  m<sup>3</sup>) occur on average every 30-50 years (Lykousis et al., 2007a). These landslides trigger tsunamis (Galanopoulos et al., 1964; Stefatos et al., 2006; Tinti et al., 2007) and induce coastal erosion by upslope retrogression (Papatheodorou and Ferentinos, 1997; Hasiotis et al., 2006). Tsunamis reaching an intensity  $\geq 4$  consequently represent a significant hazard in the western Gulf of Corinth (Beckers et al. 2017), and are documented for the last two millennia from historical

56 sources and onland geological studies (De Martini et al., 2007; Kontopoulos and Avamidis, 2003;  
57 Kortekaas et al., 2011). However, these data sets are incomplete.

58  
59 A dense grid of high-resolution seismic profiles acquired in this area (Beckers et al., 2015) was used to  
60 realize an inventory of the large mass transport deposits (MTDs) that may be interpreted as the result of  
61 submarine landslides. Dated from the Late Pleistocene and the Holocene, the mapped mass transport  
62 deposits range from  $10^6$ - $10^9$  m<sup>3</sup>. Average recurrence intervals are presented and discussed, as well as  
63 pre-conditioning factors that might have played a role in the occurrence of these large submarine  
64 landslides. The MTDs' temporal distribution is discussed, as well as the implications of their occurrence  
65 on tsunami hazard.

66  
67 **2 Setting**  
68 The western Gulf of Corinth is characterized by a relatively flat deep basin dipping gently to the east.  
69 Featuring a narrow canyon in the west ([the Mornos Canyon](#)), it widens in the east (Delphic Plateau, Fig.  
70 1). It is bordered by steep slopes on all sides (Fig. 1) To the north, it is limited by the Trizonia scarp with  
71 slopes ranging from 25° to locally more than 35° and the associated Trizonia Fault (Nomikou et al.,  
72 2011); these slopes are mostly devoid of sediments which are trapped in the bay areas to the north (Fig.  
73 1). To the south, the western Gulf is bordered by 400m high Gilbert deltas built by the Erineos,  
74 Meganitis and Selinous rivers that lie in front of the active Psathopyrgos, Kamari and Aigion Faults  
75 running along or near the coastline. Delta fronts have 15° to 35° slopes incised by gullies (Lykousis et  
76 al., 2007; Nomikou et al, 2011) and consist of a thick pile of fine grained sediments. The delta-front  
77 sediments accumulated over the Holocene and the previous glacial-interglacial period have thicknesses,  
78 respectively, larger than 50m and 100 m (Fig. 1; Beckers, 2015; Beckers et al, 2016). At the north-  
79 western end of the Gulf, lies the largest fan-delta of the Mornos River that drains 913 km<sup>2</sup> and is by far  
80 the largest watershed among the rivers flowing toward the westernmost Gulf of Corinth (Fig. 1). The  
81 delta fronts are highly unstable (Ferentinos et al, 1988; Lykousis et al., 2009), which favours frequent  
82 submarine landsliding (Stefatos et al., 2006; Tinti et al., 2007; Fig. 1). During the last centuries,  
83 submarine landslides have been triggered by earthquakes and by sediment overloading on steep slopes  
84 (Galanopoulos et al., 1964; Heezen et al., 1966). Numerous debris-flow deposits and mass-transport  
85 deposits (MTDs) have thus accumulated at the foot of the deltas (Ferentinos et al., 1988; Beckers et al.,  
86 2016; Fig. 1). Alongside these gravity-driven sedimentary processes, contour-parallel bottom-currents  
87 also influenced sediment transport in this area (Beckers et al., 2016).

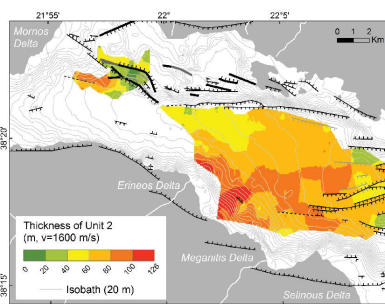
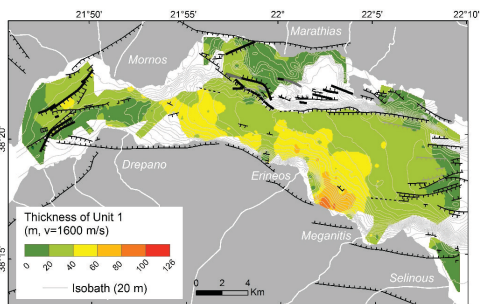
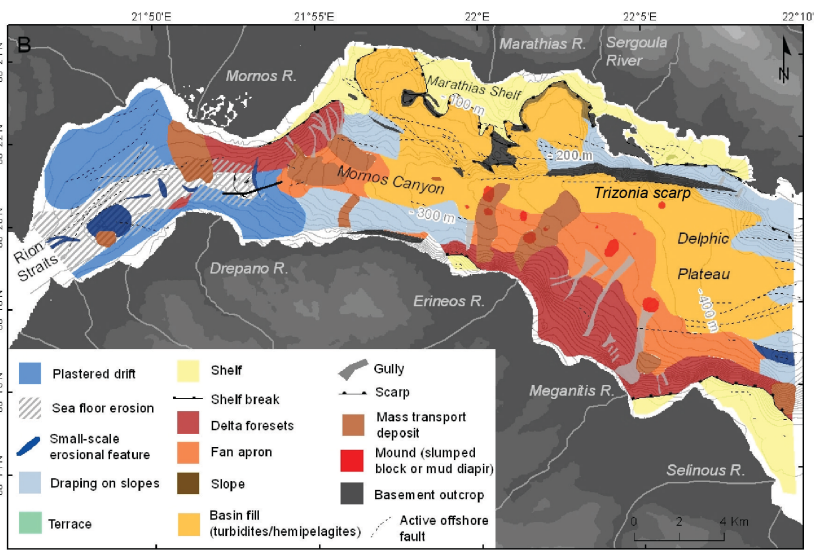
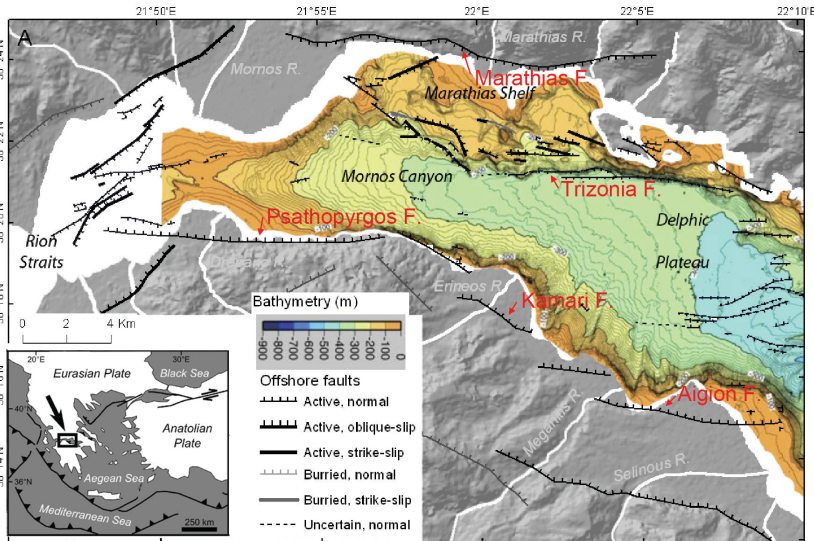
88  
89 [The shallow sedimentary infill of Gulf of Corinth infill consists of a distinct alternation between](#)  
90 [seismic-stratigraphic units with parallel, continuous high-amplitude reflections and units with parallel,](#)  
91 [continuous low amplitude reflections to acoustically transparent seismic facies \(e.g. Bell et al., 2008;](#)  
92 [Taylor et al., 2011\). Generally, the semi-transparent units are thicker than the highly reflective units \(e.g.](#)  
93 [Taylor et al., 2011\). These alternating seismic-stratigraphic units have been observed throughout the](#)  
94 [Gulf of Corinth and have been interpreted as depositional sequences linked to glacio-eustatic cycles](#)  
95 [\(Bell et al., 2008; Taylor et al., 2011\). Because of the presence of the 62 m deep Rion Sill at the entrance](#)  
96 [of the Gulf, the Gulf of Corinth was disconnected from the World Ocean during Quaternary lowstands](#)  
97 [and was thus a non-marine sedimentary environment. The marine and non-marine environments are](#)  
98 [associated with different climatic regimes \(e.g. Leeder et al., 1998\). During glacial stages, the sparse](#)  
99 [vegetation cover was more favourable to erosion than during interglacials, so high quantities of](#)  
100 [sediments were routed towards the Gulf \(Collier et al., 2000\). These lowstand deposits appear as thick,](#)  
101 [low-reflective units. The thin, high-reflective units are interpreted to represent the marine highstand](#)  
102 [deposits. The last lacustrine-marine transition has been sampled in different sedimentary cores \(Collier](#)  
103 [et al., 2000; Moretti et al., 2004; Van Welden, 2007; Campos et al., 2013\).](#)

104  
105  
106 **3 Data and Method**  
107 Two seismic reflection surveys were carried out in 2011 and 2014 with the aim of imaging the  
108 subsurface below the westernmost Gulf of Corinth floor. The data were acquired by the Renard Center

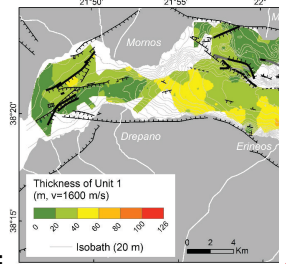
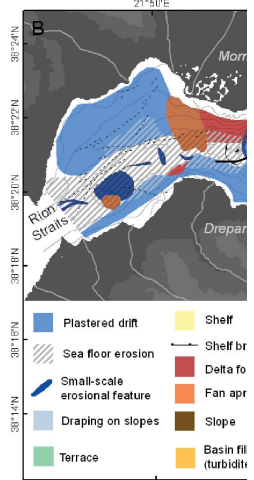
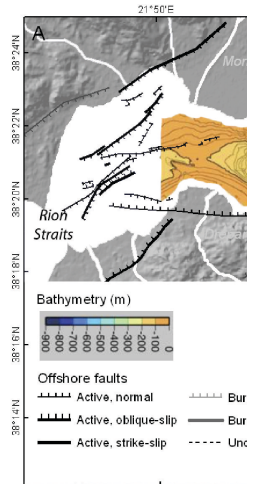
109 of Marine Geology of the University of Ghent along a grid of 600 km high-resolution seismic profiles  
110 with a "CENTIPEDE" Sparker seismic source combined with a single-channel high-resolution streamer  
111 as receiver (see details in Beckers et al., 2015, [the seismic grid is shown in Fig. 2](#)). The expected vertical  
112 resolution at depth is ~1 m. In the deep basin (Canyon and Delphic Plateau areas, Fig. 1), the maximum  
113 penetration depth below the sea floor is about 360 ms TWTT (two-way travel time) to the east and about  
114 100 ms TWTT to the west, i.e., 270-360 m and 75-100 m, respectively.  
115 The inferred stratigraphic framework (Beckers et al., 2015) permits to identify two temporal horizons.  
116 Reflector 1 has been mapped in the whole study area, except in a basin west of the Trizonia Island (Fig.  
117 [1](#)). This reflector corresponds to the beginning of the last post-glacial transgression, at 10.5-12.5 ka  
118 (Cotterill, 2006; Beckers et al., 2016). The second temporal horizon, 'reflector 2', has been mapped in  
119 the Delphic Plateau area only. It corresponds to the marine isotopic stage 6 to 5 transgression, which  
120 occurred at ca. 130 ka.  
121  
122 **Figure 1.** Study area with at the top, the fault map of Beckers et al. (2015) with the bathymetry from  
123 Nomikou et al. (2011), in the middle, the morphosedimentary map of Holocene deposits of Beckers et  
124 al. (2016), at the bottom the isopach maps of the Holocene (Right ; Beckers et al., 2016), and of the  
125 preceding period from 10 to 130 ka (Left ; Beckers, 2015). White areas in the bottom figures correspond  
126 to the ones with poor data or with an absence of stratigraphic marker. Grey curves in middle and bottom  
127 figures are sea floor contour lines interpolated from the seismic grid.

Arnaud 25/2/2018 10:46

Deleted: 2



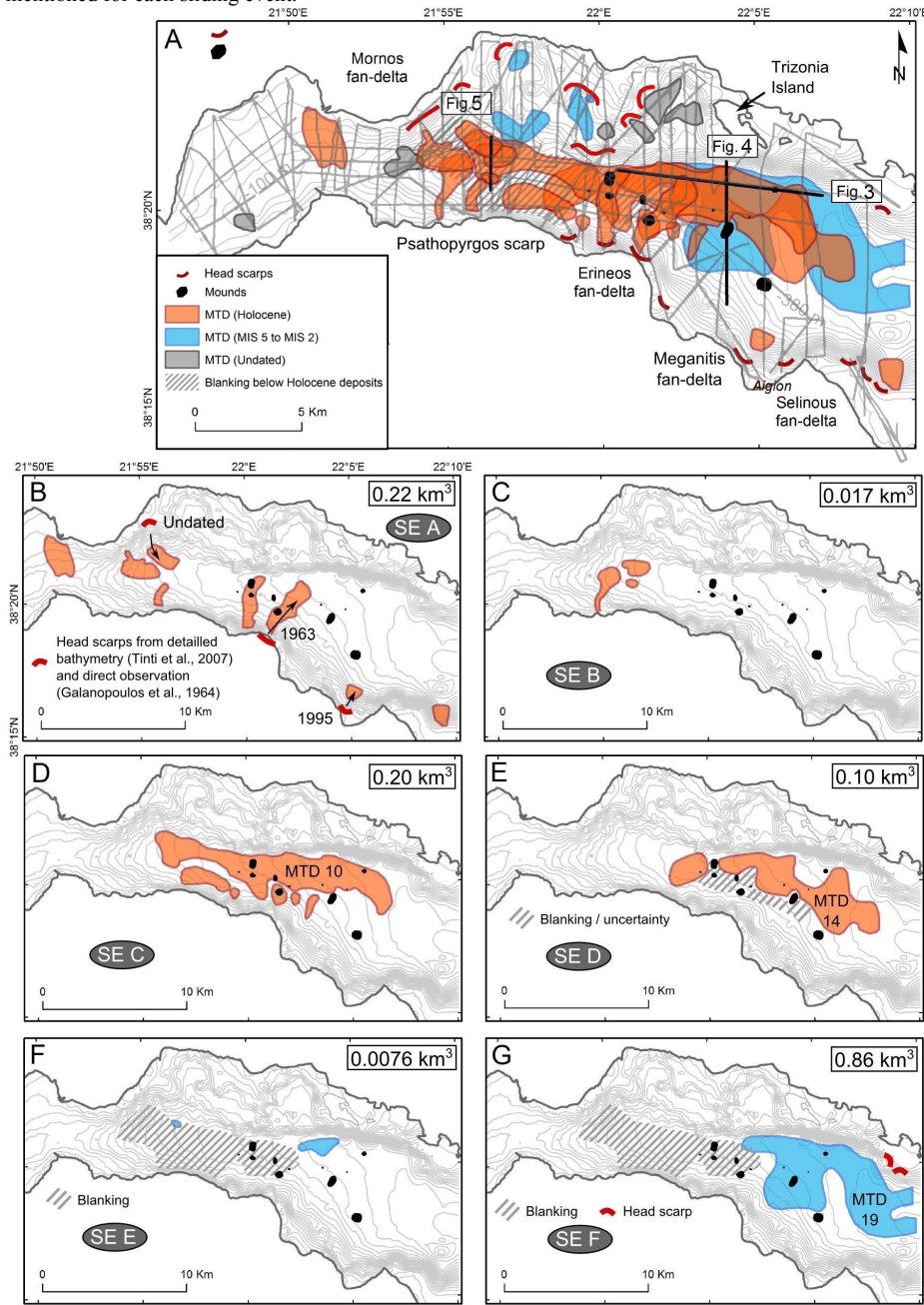
Aurélia Ferrari 5/3/2018 17:43



Deleted:

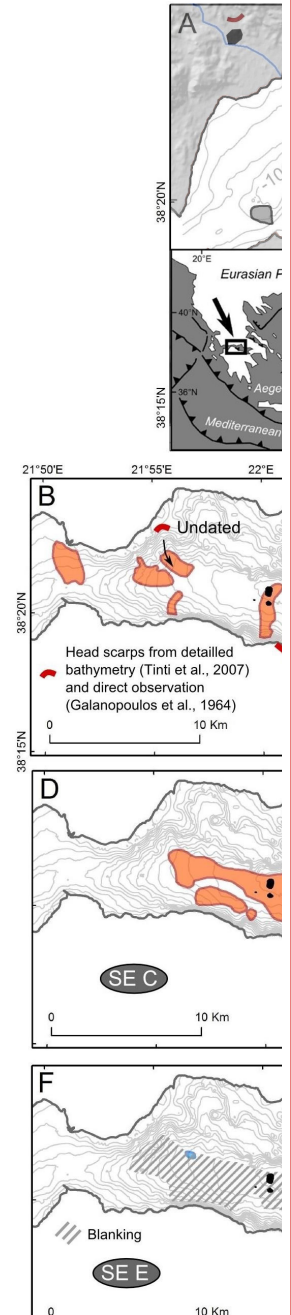


131 | **Figure 2.** Inventory of mass transport deposits (MTDs) at the westernmost Gulf of Corinth for the last ca.  
 132 | 130 ka. A) spatial extent and age of the 32 MTDs with in grey seismic grid used for the inventory; B) to G):  
 133 | spatial distribution of MTDs for each sliding event (SE). Grey lines show the seismic grid. Black dots  
 134 | represents the mounds described in Beckers et al. (2016). The total volume of sediments in the MTDs is  
 135 | mentioned for each sliding event.



136

Aurélia Ferrari 5/3/2018 17:45



Deleted:

138  
139 Mass transport deposits have been identified on high-resolution seismic profiles based on their typical  
140 seismic facies made of discontinuous to chaotic reflections. The shape of each deposit in map view has  
141 been interpolated manually, based on the seismic profiles that intersect the MTD. Thicknesses were  
142 derived using a seismic velocity of  $1600 \text{ m s}^{-1}$  (Bell et al., 2009). For the largest MTDs, an inverse  
143 distance weighted interpolation between thickness data points was used to derive isopach maps of the  
144 deposits and estimate their total volume. However, this interpolation method cannot be used for smaller  
145 MTDs crossed only by a few seismic lines. In this case, the volume was estimated by multiplying the  
146 MTD surface by an average thickness value. The derived volumes of small MTDs (surface area  $< \sim 2$   
147  $\text{km}^2$ ) are thus rough estimates, especially for MTDs crossed by only two or three seismic profiles. By  
148 contrast, volume estimates of large MTDs (surface area  $> \sim 5 \text{ km}^2$ ) are more accurate with volume  
149 uncertainties probably  $< 20 \%$ .

150  
151 Landslide headscarps have been mapped using three different data sources, namely (1) the grid of high-  
152 resolution seismic profiles acquired for this study, (2) an analysis of three submarine landslides in the  
153 study area by (Tinti et al., 2007), and (3) a 3D bathymetric view of the area between the Erineos and the  
154 Selinous fan-deltas from Lykousis et al. (2009). In the absence of multi-beam bathymetry over the  
155 whole study area, the mapping of Late Quaternary submarine landslides head scarps presented here is  
156 certainly not exhaustive. The location of potential headscarps associated with the largest MTDs mapped  
157 in the following are also discussed considering the location of the thickest deposits and the nearest  
158 upslope delta-front sediments.

#### 159 160 **4 Results**

161 Thirty-two MTDs have been imaged in the study area, from which 67% are located in the large E-W  
162 trending basin located below the flat deep basin (Mornos Canyon and Delphic Plateau, Fig. 2). Eight  
163 MTDs have been identified in the northern margin of the Gulf, and two in the Nafpaktos Bay to the west  
164 of the Corinth Gulf (Fig. 2). The age of 24 MTDs has been estimated based on the stratigraphic  
165 framework developed previously (Beckers et al., 2015): 19 of them occurred during the Holocene and 5  
166 during the period between  $\sim 130 \text{ ka}$  and  $\sim 11.5 \text{ ka}$ . A finer stratigraphy could be established in the flat  
167 deep basin, thanks to the relative continuity of the reflectors over this 20 km-wide area. Consequently,  
168 this work focuses on the 22 MTDs located in this area.

169  
170 In the Delphic Plateau basin (eastern part of the deep flat basin), most MTDs are imaged as lenticular  
171 bodies of low-amplitude, incoherent reflections (Fig. 3 and 4). They generally have a flat upper surface  
172 and pinch out on their margins. Their thickness ranges between a few meters, which is the minimal  
173 thickness for a MTD to be imaged with the seismic system used, and 53 meters. The geometry and  
174 seismic facies indicate subaquatic mass-flow deposits (e.g. Moernaut et al., 2011, Strasser et al., 2013).  
175 The seismic facies of many MTDs also suggests a fine-grained lithology. However, this statement must  
176 be viewed cautiously considering the uncertainties on the interpretation of seismic facies in terms of  
177 grain-size, especially for reworked sediments. For instance, failure of coarse-grained deltaic deposits  
178 commonly result to their total disaggregation and transformation into grain flows and turbidity currents,  
179 whereas finer grained deposits evolve as landslides and cohesive debris flows (Tripanas et al., 2008).

180  
181 In the Mornos Canyon basin (western part of the deep flat basin), the MTDs present the same general  
182 characteristics but the reflector pattern is more variable (Fig. 5). Some high-amplitude reflections and  
183 coherent layering are observed in some MTDs, suggesting coarser-grained sediments and locally  
184 preserved stratigraphy.

185  
186 Finally, some of the 22 MTDs show sediment/fluid escape features at their top (Fig. 4 and 6). Such features  
187 might have been produced by the combination of under-compaction (excess pore water pressure) and  
188 shaking, thus possibly pointing to paleoearthquakes (e.g. Moernaut et al., 2007, Moernaut et al., 2009).  
189 The volume of sediments in individual MTDs ranges from  $7.7 \cdot 10^5$  to  $8.6 \cdot 10^8 \text{ m}^3$  (Fig. 5).

190  
191 Landslide headscarps have been identified in different parts of the study area (Fig. 2A). They are  
192 particularly numerous on the slopes of the large Gilbert fan-deltas of the Erineos, Meganitis and

Aurélia Ferrari 5/3/2018 17:57

Deleted: Fig

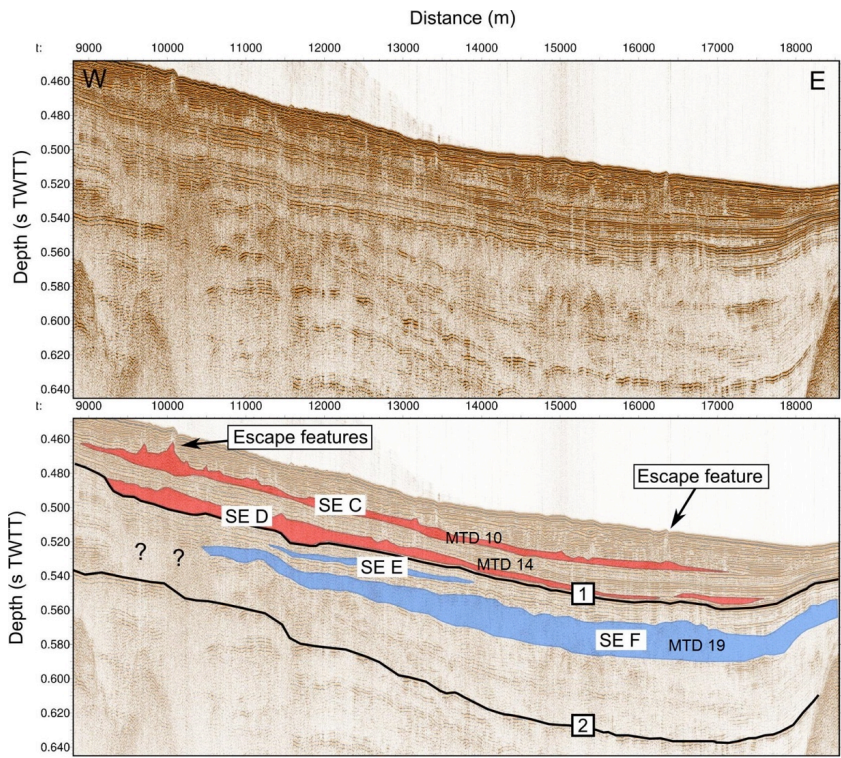
194 Selinous at the south-east and Mornos at the north-west. In the latter area, one up to 50 m-high  
195 headscarp is imaged in the seismic data. The absence of undisturbed sediments on the erosional slope,  
196 downslope of the headscarp, suggests a recent age. In the Erineos, Meganitis and Selinous fan-delta  
197 slopes, headscarps have been identified in the seismic data and on the 3D view from Lykousis et al.  
198 (2009). Most of these headscarps are relatively small, lunate-shaped features linked to gullies ([see also](#)  
199 [the bathymetric map in Fig. 1](#)). Two large head scarps are localized on the northern slope as well (Fig.  
200 2). Linking a headscarp to a particular MTD is often delicate for two reasons. First, the age of the  
201 headscarps is difficult to estimate because these erosional forms often affect steep slopes in coarse-  
202 grained deposits, making impossible to define a seismic stratigraphy in such areas. Second, at the foot of  
203 these erosional slopes, a high number of MTDs are stacked (e.g., Fig. 3). Exceptions, detailed hereafter,  
204 concern three recent submarine landslides and the largest observed MTD (MTD 19 in [sliding event F](#)).  
205

Arnaud 25/2/2018 14:01

Deleted: SE

207  
208  
209  
210  
211  
212  
213

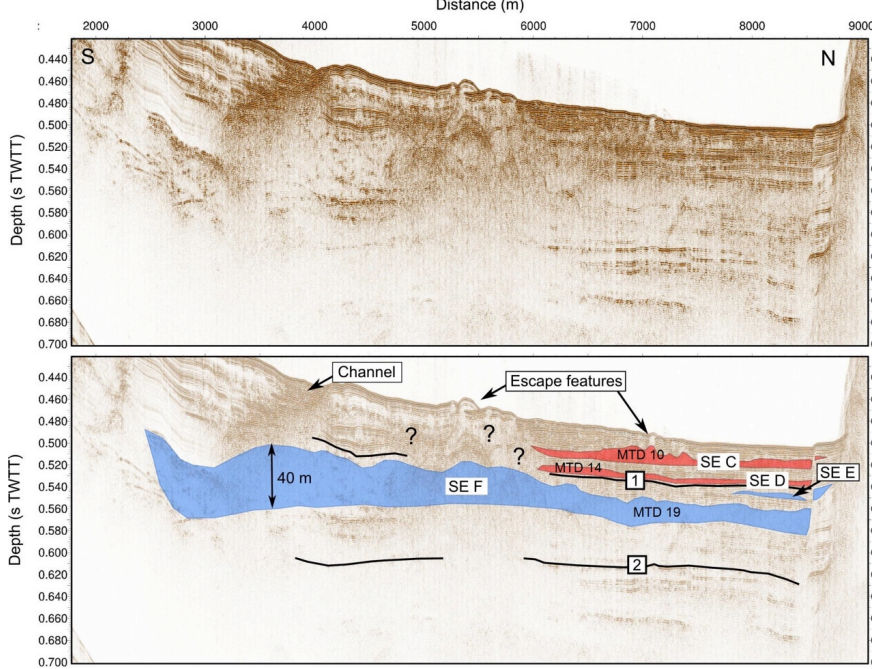
**Figure 3.** E-W Sparker seismic profile showing the mass transport deposits imaged in the Delphic Plateau basin. See the location of the profile in Fig. 2. Horizon [1] indicates the beginning of the last post-glacial transgression, at 10.5-12.5 ka and horizon [2] the marine isotopic stage 6 to 5 transgression, which occurred at ca. 130 ka (Cotterill, 2006; Beckers et al., 2015; 2016)



214  
215



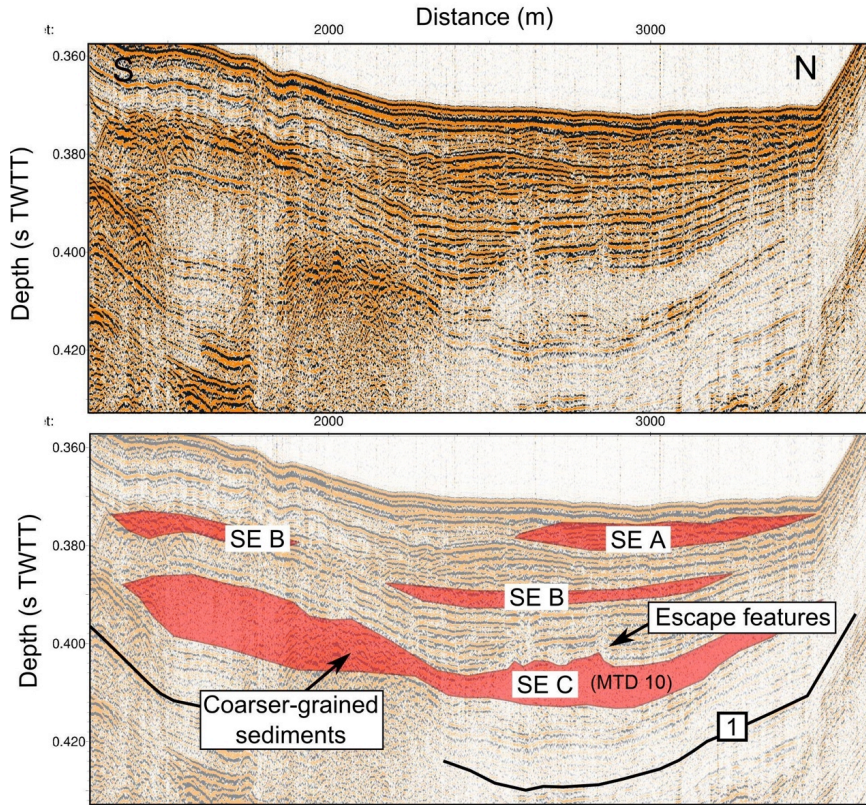
216 | **Figure 4.** S-N Sparker seismic profile showing the mass transport deposits imaged in the Delphic Plateau  
 217 basin. Questions marks highlight units of remobilized sediments that are difficult to localize in the  
 218 stratigraphic framework. See the location of the profile in Fig. 2.



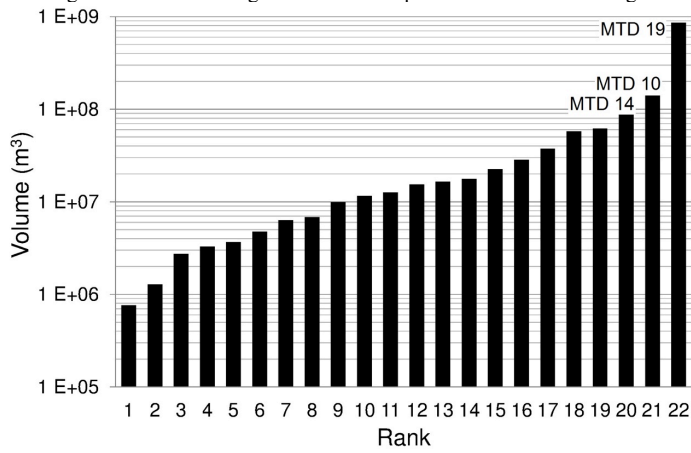
219  
 220



221 | **Figure 5.** Examples of mass transport deposits in the Canyon basin. See the location of the Sparker seismic  
 222 | profile in Fig. 2



223  
 224  
 225 | **Figure 6.** Volume distribution of the 22 MTDs studied in the Canyon and the Delphic Plateau basins. The  
 226 | names given to the three largest MTDs correspond to the notation in Fig. 2.



227  
 228  
 229

230 The stratigraphic position of MTDs in the Canyon and in the Delphic Plateau basins is not random. Most  
231 of them are clustered and are defining multi-MTDs temporal "events", based on common un-deformed  
232 underlying or overlying reflections that can be followed across the basin. Such correlations suggest that  
233 six events of large clustered submarine mass wasting occurred over the last 130 ka. Two sliding events  
234 (SE) are represented by clustered MTDs located between reflectors 2 and 1 (SE E and F). The four  
235 others occurred during the Holocene: SE D comprises MTDs deposited just on top of the reflector 1, SE  
236 C is located in the middle of the Holocene sequence, SE B somewhat higher, and finally SE A includes  
237 MTDs at or near the sea floor responsible for its present-day hummocky topography. The spatial  
238 distribution and the total volume of the MTDs associated to each of these events are represented in Fig.  
239 2.

240  
241 In some zones (Fig. 2), the existence or the geometry of MTDs is difficult to evaluate because of seismic  
242 blanking and strong chaotic reflections affecting some stratigraphic intervals. Above reflector 1, the  
243 stratigraphy is clear except regarding the southern extension of MTD 14 in SE D. The low amplitude,  
244 almost transparent reflections characterizing the MTD deposit extends until a more chaotic and thicker  
245 deposit associated with surface mounds (Fig. 4). We could not decipher if the chaotic reflections that  
246 disturb the seismic stratigraphy was associated with MTD 14 in SE D or in relation with sediment  
247 remobilization from the underlying sliding event F (Figs. 4 and 5). So the mapped extension of MTD 14  
248 in Fig. 2E is conservative and considered as a minimum. Below reflector 1, the amplitude of the  
249 reflectivity sharply decreases, which is a characteristic of lowstand deposits in the Gulf (Bell et al.,  
250 2008), and blanking occurs in two areas. In the Mornos Canyon area, a wide blanking area exists at a  
251 depth of about 50 to 70 m below the sea floor, a few meters below reflector 1, in direct continuity with  
252 the delta of the Mornos River. Blanking is thus a low-stand related feature and might correspond to  
253 coarse grained, organic rich sediments of the Mornos River. Consequently, the stratigraphy of MTDs  
254 between reflectors 2 and 1 is well established only below the Delphic Plateau. The other area associating  
255 with blanking and strongly disturbed sediments forming mounds occurs at the junction between the  
256 Mornos Canyon and the Delphic plateau at the foot of the Erineos foreset beds, at a depth similar to SE  
257 F. Its origin is unknown, but it might be related to an MTD deposit in relation with MTD 19.

258  
259 The definition of sliding events reflects a clustering of submarine landslides in a relatively short period  
260 of time. It does not necessarily imply a synchronous occurrence of all submarine landslides included in  
261 one event. Indeed, the accuracy of the correlation between separated MTDs that are interpreted to  
262 belong to the same sliding event is in the order of one or two reflections in the seismic data. Deciphering  
263 the exact MTD chronology within a sliding event was not possible because of the discontinuous  
264 character of many reflections and the relatively large distance that separates some MTDs (up to 8.5 km).  
265 This "stratigraphical" uncertainty corresponds to ~1-2 meters of sediment or, based on sedimentation  
266 rate estimates, sliding events represent a set of MTDs that occurs over a period of 300 to 1000 years  
267 (Lykousis et al., 2007).

268  
269 Individual sliding events are characterized as follows (Fig. 2B to G):

270  
271 *Sliding event A:* Eight MTDs at or near the sea floor have been identified. Their spatial distribution  
272 indicates that three of them result from slope failures in the Mornos delta and five from failures at  
273 different locations along the southern margin (Fig. 2). The volumes of these MTDs range between ~4.7  
274  $10^6 \text{ m}^3$  and ~6.2  $10^7 \text{ m}^3$ , and the total volume of the eight MTDs is about ~2.2  $10^8 \text{ m}^3$ .

275  
276 Some of these MTDs correspond to submarine landslides described in the literature (Galanopoulos  
277 1964; Papatheodorou and Ferentinos 1997; Tinti et al., 2007). The MTD located north-east of the  
278 Erineos delta results from a coastal landslide on this fan-delta in 1963, which triggered a large tsunami  
279 on both sides of the Gulf (Galanopoulos et al., 1964; Stefatos et al., 2006). The MTD located at the foot  
280 of the Meganitis fan-delta likely corresponds to a coastal landslide triggered by the 1995 Aigion  
281 earthquake on this delta (Papatheodorou and Ferentinos 1997; Tinti et al., 2007). The volumes of  
282 sediments involved in these two landslides have been estimated at ~4.6  $10^7 \text{ m}^3$  from the data presented  
283 by Stefatos et al. (2006), and about ~2.8  $10^7 \text{ m}^3$  by Tinti et al. (2007), respectively. The corresponding  
284 volumes estimated from the present study are ~6.1  $10^7 \text{ m}^3$  and ~2.2  $10^7 \text{ m}^3$ , which are in the same order

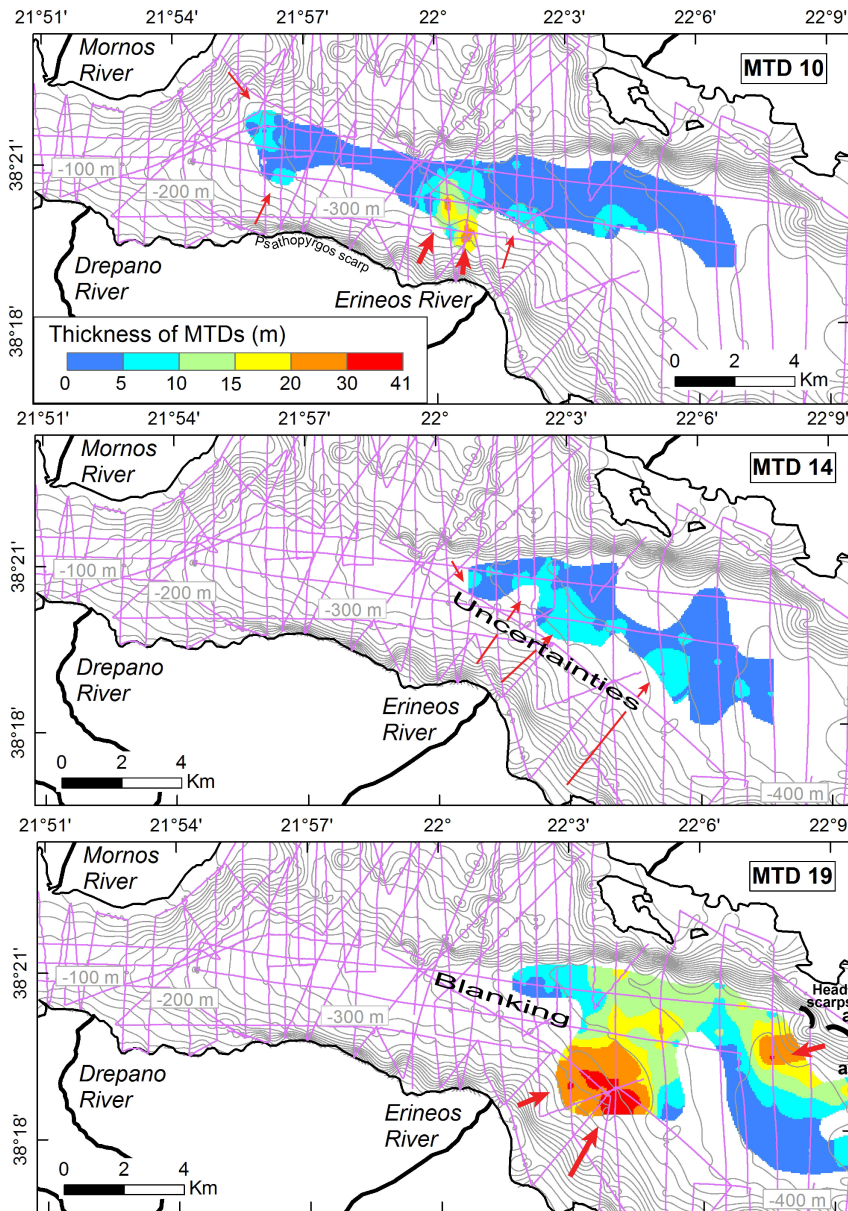
285 of magnitude. Another well preserved but undated landslide headscarp has been identified by Tinti et al.  
286 (2007) on the eastern side of the Mornos fan-delta (Fig. 2). These authors estimated the volume of the  
287 sliding mass at  $\sim 9 \cdot 10^6 \text{ m}^3$ . Our data show a MTD located about 1 km downslope of the scarp, with an  
288 estimated volume of  $\sim 9.9 \cdot 10^6 \text{ m}^3$  that fits remarkably well with the volume derived from the geometry of  
289 the scarp.

290  
291 *Sliding event B:* The sliding event B comprises three MTDs located at the western tip of the canyon.  
292 They are located between 12 and 16 m below the sea floor and are relatively thin ( $\sim 2$  to 5 m thick) (Fig.  
293 5). Location and geometry of the MTDs indicate that they result from slope failures in the Mornos fan-  
294 delta and in the Psathopyrgos scarp. The total volume of these MTDs is about  $\sim 1.7 \cdot 10^7 \text{ m}^3$ .

295  
296 *Sliding event C:* The sliding event C includes one large MTD extending over a wide area below the  
297 | [Mornos](#) Canyon and a part of the Delphic Plateau (MTD 10), and smaller deposits located at the foot of  
298 | the southern slopes, in the Psathopyrgos scarp and Erineos fan-delta areas. The thickness of MTD 10 is  
299 | shown in Fig. 7. Five local maxima are connected by a 2-5 m thick sheet of low-amplitude incoherent  
300 | reflections. The thickest sediment accumulation (30 m) is located at the foot of the Erineos fan-delta.  
301 | The other maxima are 5 to 10 m thick. Two are located at the western tip of the MTD and suggest  
302 | sediment inputs from the Mornos fan-delta area and from the Psathopyrgos scarp (Fig. 7). The last two  
303 | maxima are located in the south-eastern part of the deposit, with a possible source in the Erineos fan-  
304 | delta. The total volume that failed during sliding event C is about  $\sim 2.0 \cdot 10^8 \text{ m}^3$ , including  $\sim 1.4 \cdot 10^8 \text{ m}^3$  for  
305 | MTD 10.

306  
307 | **Figure 7.** Thickness of the largest MTDs deduced from the interpretation of Sparker seismic profiles with  
308 | probable sediment paths indicated by red arrows (bold arrow: main sources). Contours represent the sea floor  
309 | bathymetry interpolated from the Sparker data (one line every 20 m). Left: MDT 10 in sliding event C, the  
310 | largest MDT from the sliding event C. Center: Thickness of MDT 14, the largest of the two MTDs that define  
311 | the sliding event D. Bottom: The largest MTD from the presented inventory (MTD 10, sliding event F). The  
312 | black bold lines represent two landslide head scarps likely linked to the MTD. The dotted line shows the  
313 | location of the seismic profile in Fig. 8

314



315  
 316  
 317 The geometry of MTD 10 suggests that slope failures occurred simultaneously in different parts of the  
 318 westernmost gulf during sliding event C. The main source of sediment was the Erineos fan-delta, as  
 319 attested by the location of the thickest sediment accumulation in the MTD 10, and by the presence of  
 320 other MTDs at the same stratigraphic level between MTD 10 and the Erineos fan-delta (Fig. 2D).  
 321  
 322 *Sliding event D*: Two MTDs are located just on top of reflector 1 and define the sliding event D. Both  
 323 are between ~2 and 10 m thick and spread over several square kilometres in front of the Erineos and



324 Meganitis fan-deltas. The southern limit of the deposits is unclear, because the stratigraphy in the area  
325 between the two MTDs and the Erineos pro-delta is poorly constrained (hatching on Fig. 2E and  
326 question marks in Fig. 4). In this area, it is not sure whether the incoherent reflections located south of  
327 the SE D MTD at a similar depth represent the same MTD or the underlying, older (SE F), MTD or  
328 escape features from the latter, as suggested by the escape features observed at the sea floor (Fig. 4).

329  
330 The isopach map of the largest deposit (MTD 14) is shown in Fig. 7 and suggests that it was fed by  
331 slope failure(s) mostly south of the Delphic Plateau probably from the Erineos Delta Fan. The volume of  
332 MTD 14 is estimated at  $\sim 8.7 \cdot 10^7 \text{ m}^3$ , and the total volume of SE D MTDs is about  $\sim 1.0 \cdot 10^8 \text{ m}^3$ .  
333 Considering uncertainties on the geometry of these MTDs' southern edges, these values are minimum  
334 estimates.

335  
336 *Sliding event E:* Two MTDs define this sliding event. The largest one is located in the Delphic Plateau  
337 basin, just south of the Trizonia Island and has a volume of  $\sim 6.6 \cdot 10^6 \text{ m}^3$ . The second is much smaller  
338 ( $\sim 1.3 \cdot 10^6 \text{ m}^3$ ) and is located in the Mornos Canyon basin. Stratigraphically, both are located a few  
339 meters below reflector 1. However, they are horizontally 8.5 km apart, making the correlation uncertain.  
340 The total volume of the two MTDs in sliding event E is  $\sim 7.9 \cdot 10^6 \text{ m}^3$ .

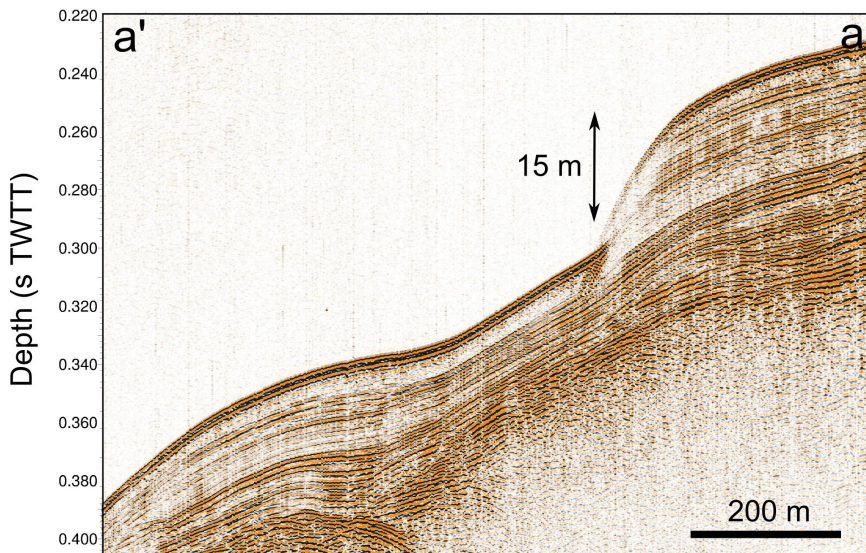
341  
342 *Sliding event F:* The sliding event F is defined by one single large complex MTD (MTD19) (Fig. 2).  
343 This deposit is located in the Delphic Plateau basin. Stratigraphically, it belongs to the upper part of the  
344 unit between reflectors 2 and 1, suggesting that this event occurred during the last glacial period. With a  
345 volume of  $\sim 8.6 \cdot 10^8 \text{ m}^3$ , this deposit is the largest MTD of the present inventory. It covers an area of 41  
346  $\text{km}^2$ , i.e., almost the whole Delphic Plateau. The isopach map reveals a main up to 40 m-thick sediment  
347 accumulation in the south-western part of the deposit (Fig. 4 and 7) and another  $\sim 30$  m-thick depocenter  
348 in the north-eastern part (Fig. 7). The MTD is imaged as low amplitude, almost transparent chaotic  
349 reflections except in the thickest part where high-amplitude reflections could indicate coarser-grained  
350 sediments and locally preserved layering (Fig. 4). No sedimentological structure has been observed in  
351 the seismic profiles between the two maxima in thickness.

352  
353 The geometry of the deposit and the absence of clear structure between the two depocenters support the  
354 idea of at least two simultaneous slope failures having generated this large MTD. The largest failure  
355 occurred south of the MTD, on the Meganitis or the Erineos fan-delta slopes. Considering the large  
356 volume of sediments in the south-western part of the MTD, we expected a major scar across the  
357 southern slopes, which we could not retrieve however neither from the seismic data, nor from published  
358 bathymetries (Lykousis et al., 2009; Nomikou et al., 2011, see our Fig. 1). Indeed, dozens of small head  
359 scarps and gullies dissect the slopes of the offshore Erineos and Meganitis deltas, making difficult the  
360 identification of large features. The second depocenter occurs near the north-eastern edge of the Delphic  
361 Plateau Basin, and upslope two submarine landslide headscarps located 2 km from each other were  
362 evidenced in seismic profiles (bold lines in Fig. 7). Cut through stratified hemipelagites, they are 11 and  
363 15 m-high and are located at 300 and 195 m below the sea level, respectively (Fig. 7). Although it is not  
364 possible to reconstruct the 3D geometry of a single large headscarp from the seismic data, this would be  
365 a good candidate source of the thick sediment accumulation in the north-eastern part of MTD 19.

366  
367 **Figure 8.** Sparker seismic profile illustrating a submarine landslide head scarp that is probably linked to the  
368 MTD 19. See the location of the profile in Fig. 7.

369





370  
371  
372  
373  
374  
375  
376  
377  
378  
379  
380  
381  
382  
383  
384  
385  
386  
387  
388  
389  
390  
391  
392  
393  
394  
395  
396  
397  
398  
399  
400  
401  
402  
403  
404

## 5 Discussion

### 5.1 Limitations of the analysis

Before discussing the implications of the presented MTD inventory in the deep flat basin in terms of sediment sources and triggering mechanisms, it is necessary to point out that only submarine landslides that have remobilized a sufficient quantity of sediments down to the basin floor are considered here. Moreover, the high-resolution seismic profiling system used does not permit identifying MTDs thinner than ~1 m. Consequently, our inventory is incomplete and could be refined by the use of very-high resolution seismic profiling systems and long cores.

### 5.2 Sediment sources

According to the mapping of the thickness of the deposits, large sliding events in the westernmost Gulf of Corinth mainly result from slope failures in, or close to, the Gilbert-type fan-deltas. Large sediment volumes were trapped in these deltas during the Holocene. As shown in Figure 1, Holocene foreset beds reach 40 to 60 m in thickness on average in the Eroneos and Meganitis fan-deltas, and sediment accumulation during the Holocene exceeding 100 m have been observed locally in between. These are the sources of MTD 10 in sliding event C and MTD 14 in sliding event D. The remarkable amount of sediments delivered to the gulf of Corinth during the Holocene probably results from large volumes of sediments stored onland during the last glacial period that were mobilized from river floodplains and colluvial deposits to rivers deltas. Widespread soil erosion resulting from human deforestation and agriculture during the second half of the Holocene also contributed to increase sediment fluxes in this period. Similarly, the previous period considered here spanning ~130 ka to ~11 ka is also characterized by a large sediment accumulation with a pile of 60 to 120 m forming the delta fronts of the Erineos and Meganitis delta (Fig. 1). These sources are some of the main source of MTD 19 in sliding event F.

The seismic facies of most large MTDs also implies that they are likely composed mainly of fine-grained sediments, and seismic profiles across fan-delta area have shown that the pro-delta foresets are locally made of a thick accumulation of stratified fine-grained sediments. These fan-delta sediments are probably the main source of sediments for the largest MTDs (MTD 10, 14 and 19). However, some smaller MTDs seem to be made of coarser-grained sediments according to the seismic character (e.g., in

Arnaud 25/2/2018 14:51

Deleted: 100

Arnaud 25/2/2018 14:52

Deleted: one

Arnaud 25/2/2018 14:50

Deleted: 0

408 | SEs A and B in the [Mornos](#) Canyon basin), suggesting failure also occurred in coarser-grained parts of  
409 the fan-deltas located at the junction between the topset and the foreset beds (e.g., the 1963 slide in the  
410 Erineos fan-delta).

411

### 412 5.3 Significance of the sliding events

413

414 The data suggest that large submarine landslides have been triggered during six short periods of time  
415 over the last 130 ka. These sliding events include variable numbers of clustered MTDs, from one (SE F)  
416 to 8 (SE A). During three sliding events (C, D, F), a particularly large MTD accumulated at the basin  
417 floor, and it has been shown that these large MTDs resulted from several possibly synchronous slope  
418 failures. Similar MTD distributions have been observed in lakes in the Alps and in the Chilean Andes  
419 (Strasser et al., 2013; Moernaut et al., 2007). In these studies, the correlation of MTDs into a same  
420 "sliding event" was supported by radiocarbon dating and a simultaneous triggering has been proposed.  
421 Correlations between the mass wasting records of neighbour lakes and the historical seismicity revealed  
422 that most of these "sliding events" had been triggered by large earthquakes (Strasser et al., 2006;  
423 Moernaut et al., 2007). In the westernmost Gulf of Corinth, neither coring, nor dating is available to  
424 confirm our correlations between MTDs. Moreover, the occurrence of frequent turbidity currents  
425 (Heezen et al., 1966; Lykousis et al., 2007a) and small-scale submarine landslides perturbs the sediment  
426 layering and induces discontinuities in the seismic reflections, which makes MTD correlations based on  
427 the seismic stratigraphy less accurate there than in many lakes.

428

429 The case of sliding event A demonstrates that MTDs grouped within the same event did not necessarily  
430 occur at the same moment. Indeed, direct observation has shown that one MTD of this event occurred in  
431 1963 AD and another in 1995 AD. By contrast, the synchronicity of different submarine landslides has  
432 been suggested for SE C, D and F from the complex shape of the large MTDs they include. Though not  
433 a proof, this lends support to the hypothesis of a seismic trigger of these three sliding events.

434

435 Consequently, the sliding events defined in this study may represent two different situations. In a first  
436 case, they correspond to a period of time of 0.3 to 1 ka during which several submarine landslides of  
437 various origins occurred. The sliding event A is such a case, with the coastal landslide caused in the  
438 Megaritida delta area by the 1995 Aigion earthquake and an aseismic coastal landslide in the Erineos  
439 delta area in 1963. The second case refers to likely simultaneous submarine landslides originating from  
440 different slopes and forming a wide MTD of complex shape in the basin floor. An example of this case,  
441 which is proposed to be earthquake-triggered, is the sliding event F, with a single MTD of complex  
442 shape. Sliding events C and D possibly belong to this category as well. There is insufficient data to  
443 allow for the determination of the nature of the minor events B and E.

444

445 Two main questions arise from these observations.

- 446 - Is seismicity the only forcing of SEs C, D and F or could other triggers or pre-conditioning factors
- 447 such as sediment supply and sea level change have influenced the system?
- 448 - What are possible trigger mechanisms and/or pre-conditioning factors responsible for a cluster of slope
- 449 failures such as SE A?

450

451 Urlaub et al. (2013) make inferences about controls on triggers of submarine landsliding from the  
452 statistical analysis of the ages of 68 very large slides ( $> 1 \text{ km}^3$ ) around the world. From a subset of 41  
453 slides that occurred during the best documented last 30 ky, they show that the distribution of number of  
454 events per ky resembles a Poisson distribution, suggesting that large submarine mass wasting might be  
455 essentially random or, at best, that the global-scale signal for a climatic control, through either sea level  
456 or sedimentation rate changes, is incoherent (non-uniform response of continental slopes worldwide) or  
457 too weak to be expressed clearly with such a small sample size. They also note that, though strong  
458 earthquakes might represent a temporally random trigger at the global scale, most of the slides in their  
459 data set are located in low-seismicity passive continental margins (Urlaub et al., 2013). Here, we first  
460 investigate the possible role of earthquakes through a comparative analysis of the frequency of sliding  
461 events and earthquakes in the Gulf of Corinth area. Then, other potential controls will be discussed by  
462 comparing the age distribution of the largest sliding events with published data about changes in

463 sediment dynamics and marine conditions in the Corinth Rift area. Owing to the small number of events  
464 and high age uncertainties, which rule out statistical considerations, we provide only a qualitative  
465 analysis.

#### 466 5.4. The possible role of large earthquakes

467 The last four sliding events occurred during the last 10-12 ka, at an average rate of one event every 2.5-3  
468 ka. Only two sliding events have been detected between ca. 130 ka and 10-12 ka. This high Holocene  
469 frequency compared with the ~120 kyrs anterior period may be attributed to two factors. First it might  
470 be a bias, because the seismic reflections corresponding to the last glacial period (110-12ka) are less  
471 clear (lower amplitude and lower continuity) than the reflections from the Holocene interval.  
472 Consequently, medium-sized landslides such as those detected in SEs A and B might have been missed  
473 in the seismic unit between reflectors 2 and 1. Second, it could be attributed to a change in earthquake  
474 frequency due to a Holocene acceleration of the strain rates that was evidenced by fluvial morphometry  
475 (Demoulin et al., 2015) and subsidence markers (Beckers, 2015).

476 The average recurrence interval for large earthquakes (Mw 6-7) has been estimated in the central part of  
477 the Gulf of Corinth at ~500 yr during the Holocene, and ~400 yr for the period 12-17 ka, based on the  
478 record of "homogenites" in the deepest part of the Gulf (Campos et al., 2013). In the western Gulf of  
479 Corinth, estimates from palaeoseismological trenches on individual faults suggest an average recurrence  
480 interval  $\leq 360$  yr on the Aigion fault (Pantosti et al., 2004), and of 200-600 yr on the East Helike fault  
481 (McNeill et al., 2005) for the past 0.5-1 ka. It is clear, therefore, that large sliding events in the  
482 westernmost Gulf of Corinth were less frequent than Mw 6-7 earthquakes, during both the Holocene and  
483 the last glacial period. Consequently, while (anomalously?) large earthquakes could have triggered SEs  
484 C, D and F, as suggested above from the geometry of MTDs 10, 14 and 19, it is likely that other factors  
485 contributed to the occurrence of such large sliding events. These factors are explored in the next section.

#### 486 5.5 Other potential triggers and pre-conditioning factors

487 Other possible processes that might have "pre-conditioned" or triggered sliding events in the Gulf of  
488 Corinth need to show a return period of at least 2.5 ka over the last 12 ka in order to fit the SE  
489 frequency. The following processes are proposed:  
490 1. Sediment loading on top of a weak layer (e.g., gas-filled muddy sediments, as suggested for the area  
491 by Lykousis et al. (2009)) (pre-conditioning factor);  
492 2. Pulses of increased onshore erosion inducing temporary increase of sedimentation offshore, in turn  
493 leading to slope overloading (pre-conditioning factor);  
494 3. Sea level changes, which would have favoured slope failures during either lowstand conditions  
495 (Perissoratis et al., 2000) or sea level rises (Zitter et al., 2012) (pre-conditioning factor);  
496 4. Changes in the circulation and/or intensity of bottom-currents progressively destabilizing submarine  
497 slopes through an increase in sedimentation or erosion rate (pre-conditioning factor);  
498 5. Middle-term tectonic pulses, which would have temporarily increased the level of regional seismicity  
499 (Koukouvelas et al., 2005; Demoulin et al., 2015) (trigger);  
500 6. Loading by exceptional storm waves (trigger);  
501 7. Large supply of coarse-grained sediments at a river mouth during exceptional flooding events  
502 inducing slope failures by sediment overloading, as attested for the 1963 coastal landslide on the Erineos  
503 fan-delta by Galanopoulos et al. (1964) (trigger).

504 All these hypotheses are not directly testable. Moreover, it is likely that different pre-conditioning  
505 factors and triggers have interacted in various ways over the last 130 ka. Nevertheless, the four proposed  
506 pre-conditioning factors can be discussed by comparing the SE age distribution with independent data  
507 available for the region. We focus on the four events that mobilized a large volume of sediment ( $\geq 10^8$   
508 m<sup>3</sup>, SEs A, C, D, and F) because they probably indicate slope failures in different parts of the  
509 westernmost Gulf, thus pointing to a regional signal. Even though these events have not been directly  
510 dated by coring, ages can be reasonably inferred from the seismic stratigraphy. The most recent sliding  
511 event (SE A) comprises MTDs at or near the sea floor and consequently occurred in the last 0.3-1 ka (a

Aurélia Hubert-Ferrari 23/2/2018 11:51

Deleted: a priori surprising low

Aurélia Hubert-Ferrari 23/2/2018 11:55

Deleted: during the last glacial period (110-12 ka) with respect to the Holocene might actually be somewhat

Aurélia Hubert-Ferrari 23/2/2018 11:55

Deleted: ed by the fact that

Aurélia Hubert-Ferrari 23/2/2018 11:55

Deleted: that

524 range accounting for the thin layer of hemipelagites possibly covering some MTDs). Sliding event C  
525 likely dates from the Mid-Holocene (~6-7 ka) according to the Holocene age-depth curve in the central  
526 part of the Gulf of Corinth (Campos et al., 2013). The two MTDs defining SE D occurred just after the  
527 lacustrine to marine transition at the end of the Last Glacial, around 10-12 ka. Finally, the sliding event  
528 F dates from sometime in the last glacial period.

529  
530 Among the listed pre-conditioning factors, onshore erosion dynamics in the Corinth Rift area is the best  
531 temporally documented. Fuchs (2007) presents the evolution of sedimentation rates in colluvial deposits  
532 on the southern shoulder of the Corinth Rift, in the Philiou Basin, for the last 10 ka (Fig. 9). He  
533 identifies two main phases of land degradation between 6.5 and 8.5 ka, and from ~4 ka onwards. While  
534 the age of SE A corresponds to the end of the most recent period of land degradation, the much more  
535 uncertain age of SE C could correspond to the end of the land degradation phase at 6.5-8.5 ka (Fig. 9).  
536 The sliding event D is too old to be compared with the results of Fuchs (2007). In brief, a relation might  
537 exist between periods of high sediment supply from the watersheds and the occurrence of sliding events  
538 during the last 10 kyr (hypotheses 1 and 2).

539  
540 Less information is available about Late Pleistocene sediment dynamics in the area. Collier et al. (2000)  
541 suggest that the denudation rate at the eastern end of the Gulf in the Alkyonides Basin during the last  
542 glacial period (12-70 ka) was almost twice those of the Holocene and MIS 5 interglacials. Instead, six  
543 radiocarbon dates on long cores in the center of the Gulf of Corinth show a moderate increase in  
544 sedimentation rate between the end of the last glacial period (17- 12 ka) and the Holocene (Campos et  
545 al., 2013). Overall, these data suggest that the Last Glacial probably experienced the largest  
546 sedimentation rates over the last 130 ka in most of the Gulf of Corinth. This inference is however not  
547 valid at the western tip of the Gulf. The comparison between isopach maps of the Holocene and the  
548 anterior 130-12 kyrs period evidences a large Holocene increase in sedimentation accumulation rate  
549 (Fig. 1). In the Delphic plateau basin, average sedimentation rate (excluding the thickness of MTDs)  
550 reaches ~2.4 mm/yr for the Holocene and ~0.4 mm/yr for the previous 120 kyrs. This is in line with the  
551 fact that only one large sliding event F was recorded during the ~60 ky-long Last Glacial. Increased  
552 sedimentation is thus a pre-conditioning factor of landsliding in the western Gulf.

553  
554 Beside changes in erosion rates in the watersheds, the offshore realm underwent large changes between  
555 the last glacial period and today. From 70 to 12 ka, the Gulf of Corinth was a lake and the water level  
556 was around -60 m, assuming a constant depth of the Rion Sill over this period (Perissoratis et al., 2000).  
557 During this lowstand period, the extent of submarine slopes where submarine landslides can initiate,  
558 were not significantly reduced, because the foreset beds of the Erineos and Meganitis that are the largest  
559 source of mass wasting sediments for the Delphic plateau extend down to the ~300 m isobaths. The  
560 steepest slopes of these two prodeltas are located above isobaths -100m and between isobaths -150m and  
561 -200m according to the slope map of Nomikou et al. (2011), so unstable slopes above -60m that were  
562 submerged only in the postglacial period cover a restricted area. At 10-12 ka, the rising waters in the  
563 Ionian Sea flooded the "Lake Corinth" through the Rion Sill (Moretti et al., 2003; VanWelden 2007).  
564 The sea level continued to increase from ca. -60 m to its present elevation until 5.5-6 ka, and bottom  
565 currents appeared in the study area (Beckers et al., 2016). The deposition of SE D occurred at 10-12 ka,  
566 when the water level started to increase in the Corinth Gulf. Water level change might change the stress  
567 field and pore pressure potentially affecting the earthquake cycle. Water level increase and bottom  
568 current initiation would also favoured the destabilization of sediments deposited during the preceding  
569 glacial period. In the Sea of Marmara, observations by Zitter et al. (2012) and Beck et al. (2007) show  
570 an increase in large mass wasting events at the end of the last lacustrine period and at the beginning of  
571 the marine period that likewise can be explained by a change in oceanographic conditions, confirming  
572 the possible control of these pre-conditioning factors on SE D.

573  
574  
575 **Figure 9.** Comparison between the erosion dynamics over the last 10 ka from colluvial and alluvial archives  
576 in the Peloponnese (Fuchs, 2007), the rate of local water level changes, and the occurrence of large sliding  
577 events in the westernmost Corinth Rift during the Holocene. Bars without error bars in the second panel  
578 indicate minimum sedimentation rates.

Aurélia Hubert-Ferrari 23/2/2018 12:00

Deleted: , 25 km south of Xylocastro

Arnaud 25/2/2018 22:15

Deleted: On the unstable foreset beds clearly imaged between Erineos and Meganitis fans the

Arnaud 25/2/2018 22:07

Deleted: sediment recharge

Arnaud 25/2/2018 22:15

Deleted: 8

Arnaud 25/2/2018 22:16

Deleted: 1

Aurélia Hubert-Ferrari 23/2/2018 12:28

Deleted: While the occurrence of the major SE F during this period again lends support to i

Aurélia Hubert-Ferrari 23/2/2018 12:28

Deleted: as

Aurélia Hubert-Ferrari 23/2/2018 12:29

Deleted: , it may however be surprising that no other large sliding event has been recorded under such circumstances during the ~60 ky-long Last Glacial.

Aurélia Ferrari 23/2/2018 14:34

Deleted: e

Arnaud 25/2/2018 22:23

Deleted: slide sources

Aurélia Ferrari 23/2/2018 14:35

Deleted: gulf submarine morphology was not significantly different

Aurélia Ferrari 23/2/2018 14:35

Deleted: T

Aurélia Ferrari 23/2/2018 14:35

Deleted: with

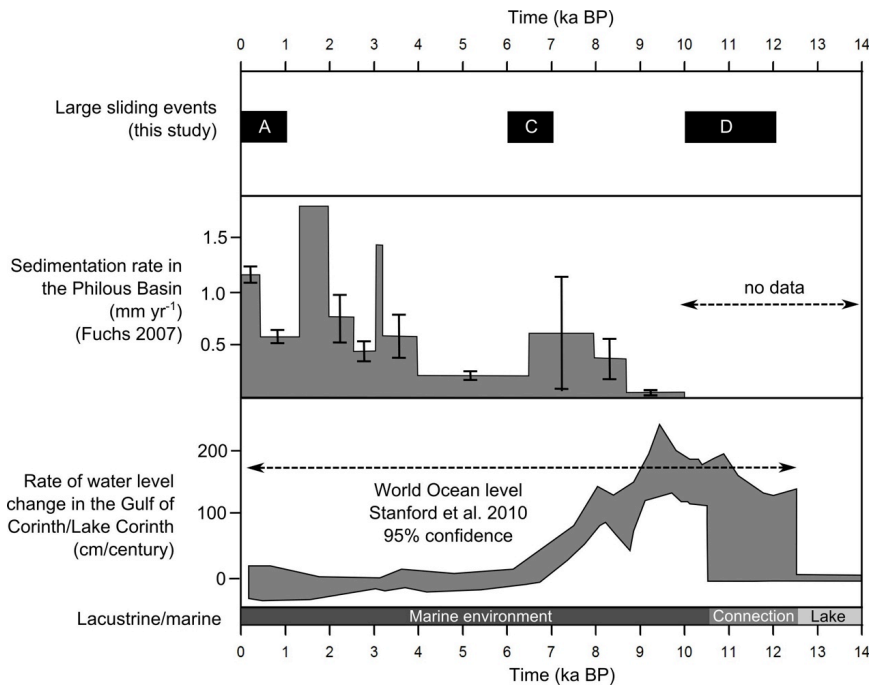
Arnaud 25/2/2018 22:24

Deleted: Its t

Aurélia Hubert-Ferrari 23/2/2018 12:31

Deleted: might have





603  
604  
605  
606

### 5.6 Conceptual model for the sliding events

607

608 Large sliding events (total volume  $\geq 10^8 \text{ m}^3$ ) occurred in the westernmost Gulf of Corinth with fairly  
609 long recurrence intervals,  $\geq 2.5 \text{ ka}$ . We suggest that their temporal distribution is primarily controlled by  
610 changes in pre-conditioning factors, which were a prerequisite for any landslide trigger to be effective.  
611 In other words, the clustering of slope failures during distinct sliding events would depend on the  
612 appropriate state of pre-conditioning factors, which occur only during limited periods of time. Two  
613 types of pre-conditioning factors may have played a significant role, on one hand increased denudation  
614 rates, identified at 17-70 ka, 6.5-8.5 ka and 0-4 ka and, on the other hand, dramatic changes in  
615 oceanographic conditions that occurred at 10-12 ka. More generally, the SE frequency would reflect the  
616 time needed to reload submarine slopes beyond their stability threshold after each event. Once the pre-  
617 conditioning factor evolution has made the slopes prone to sliding, each individual sliding event is  
618 characterized by either simultaneous submarine landslides producing large coalesced MTDs and  
619 pointing to a likely seismic trigger (SEs C, D and F) or separate smaller slides caused by various lower-  
620 intensity triggers (earthquakes, exceptional onshore flood events, as exemplified by the 1995 and 1963  
621 coastal landslides, respectively) over a few centuries (SE A).

622

623 Finally, we underline that the sliding processes have not been clearly identified in this study. Lykousis et  
624 al. (2009) mention debris flows and avalanches for slope failures on steep fan-delta slopes ( $2-6^\circ$ ) in the  
625 western Gulf of Corinth, and rotational slumps on low angle ( $0.5-2^\circ$ ) prodelta slopes. One sharp head  
626 scarp identified in this study also shows that at least one translational slide happened in hemipelagites  
627 accumulated far from the main river outlets.

628

### 5.7 Implications for tsunami hazard in the Gulf of Corinth

629  
630



631 Among the 32 MTDs identified in this study, MTD 19 stands out as a particularly large feature (a little  
632 less than 1 km<sup>3</sup> in volume). This is 6 times the volume of the second largest MDT identified in this  
633 study, and about two orders of magnitude larger than the range previously proposed for the size of  
634 submarine landslides in the westernmost Gulf of Corinth (Lykousis et al., 2007). It is also 6 times larger  
635 than the largest MTD reported in the rest of the Gulf of Corinth, which occurred in the area of the  
636 Perachora Peninsula (Papatheodorou et al., 1993; Stefatos et al., 2006). MTD 19 likely resulted from the  
637 coalescence of at least two probably synchronous major slides. If correct, these slides should have  
638 triggered very large tsunamis waves, probably larger than those reported by historical sources in the  
639 westernmost Gulf of Corinth, which were triggered by small to medium-sized slope failures  
640 (Papadopoulos 2003; Stefatos et al., 2006; Tinti et al., 2007).

## 641 642 **6 Conclusion**

643 We documented the existence of large mass wasting events during the Holocene and the Late  
644 Pleistocene in the westernmost Gulf of Corinth. Mass wasting events consist in submarine or coastal  
645 landslides that occurred during short periods of time. Six large mass wasting events are listed, their  
646 associated deposits locally representing 30% of the sedimentation since 130 ka in the Delphic Plateau  
647 Basin. In the case of large MTDs (up to almost 1 km<sup>3</sup> for the largest), a simultaneous triggering of  
648 separate slope failures is proposed, suggesting a seismic origin. However, it is suggested that the  
649 temporal distribution of sliding events is primarily controlled by the evolution of pre-conditioning  
650 factors. Two main pre-conditioning factors are identified, namely (1) the time needed to slope reloading  
651 after an event, which varied in relation with temporally varying sedimentation rates, and (2) dramatic  
652 changes in water depth and water circulation that occurred 10-12 ka ago during the last post-glacial  
653 transgression. Finally, it is likely that these sliding events have triggered large tsunami waves in the  
654 whole Gulf of Corinth, in some cases (much?) larger than those reported in historical sources.

655  
656 Competing interests. The authors declare they have no conflict of interest.

657  
658 Acknowledgement. This work has been funded within the ANR SISCOR project directed by Pascal  
659 Bernard, at Institut de Physique du Globe (Paris) and by FNRS- Grant for Researchers (CC) ID  
660 14633841. Arnaud Beckers's PhD grant was supported by the Belgian FRIA. Funding for Arnaud  
661 Beckers' stays in the ISTERre Laboratory was provided by a grant from la Région Rhône-Alpes. The  
662 authors warmly acknowledge R/V ALKYON's crew, Koen De Rycker (RCMG), and Pascale Bascou  
663 (ISTerre) for technical support, and the whole SISCOR scientific team for fruitful discussions.

## 664 665 **References**

- 666  
667  
668 Beck, C., Mercier de Lépinay, B., Schneider, J.-L., Cremer, M., Cagatay, N., Wendenbaum, E.,  
669 Boutareaud, S., Ménot, G., Schmidt, S., Weber, O., Eris, K., Armijo, R., Meyer, B., & Pondard, N.  
670 (2007). Late Quaternary co-seismic sedimentation in the Sea of Marmara's deep basins. *Sedimentary*  
671 *Geology*, 199 (1-2), 65-89.
- 672  
673 Beckers, A., Hubert-Ferrari, A., Beck, C., Bodeux, S., Tripsanas, E., Sakellariou, D., & De Batist, M.  
674 (2015). Active faulting at the western tip of the Gulf of Corinth, Greece, from high-resolution seismic  
675 data. *Marine Geology*, 360, 55-69.
- 676  
677 Beckers, A., 2015, Late quaternary sedimentation in the western gulf of Corinth : interplay between  
678 tectonic deformation, seismicity, and eustatic changes, PhD thesis, pp. 260.
- 679  
680 Beckers, A., Beck, C., Hubert-Ferrari, A., Tripsanas, E., Crouzet, C., Sakellariou, D., Papatheodorou, G.  
681 & De Batist, M. (2016). Influence of bottom currents on the sedimentary processes at the western tip of  
682 the Gulf of Corinth, Greece. *Marine Geology*, 378, 312-332.
- 683  
684 Beckers, A., Beck, C., Hubert-Ferrari, A., Reyss, J. L., Mortier, C., Albini, P., Rovida, A., Develle, A.-  
685 L., Tripsanas, E., Sakellariou, D., Crouzet, C. & Scotti, O. (2017). Sedimentary impacts of recent

686 moderate earthquakes from the shelves to the basin floor in the western Gulf of Corinth. *Marine*  
687 *Geology*, 384, 81-102.

688 Bell, R. E., McNeill, L. C., Bull, J. M., & Henstock, T. J. (2008). Evolution of the offshore western Gulf  
689 of Corinth. *Geological Society of America Bulletin*, 120, 156-178.

690 Briole, P., Rigo, A., Lyon-Caen, H., Ruegg, J., Papazissi, K., Mitsakaki, C., Balodimou A., Veis G.,  
691 Hatzfeld F., and Deschamps A. (2000). Active deformation of the Corinth rift, Greece: Results from  
692 repeated Global Positioning System surveys between 1990 and 1995. *Journal of geophysical research*,  
693 105 (B11), 25605-25625.

694 Campos, C., Beck, C., Crouzet, C., Carrillo, E., Welden, A. V., & Tripsanas, E. (2013). Late Quaternary  
695 paleoseismic sedimentary archive from deep central Gulf of Corinth : time distribution of inferred  
696 earthquake-induced layer. *Annals of Geophysics*, 56 (6), 1-15.

697  
698  
699 Collier, R. E., Leeder, M. R., Trout, M., Ferentinos, G., Lyberis, E., & Papatheodorou, G. (2000). High  
700 sediment yields and cool, wet winters: Test of last glacial paleoclimates in the northern Mediterranean.  
701 *Geology*, 28, 999-1002.

702  
703 Cotterill, C. (2006). A High-resolution Holocene Fault Activity History of the Aigion Shelf, Gulf of  
704 Corinth, Greece. PhD thesis, PhD Thesis, University of Southampton.

705  
706 De Martini, P., Pavlopoulos, K., Pantosti, D., & Palyvos, N. (2007). 3HAZ Corinth Deliverable 73:  
707 Dating of paleo-tsunamis. Tech. rep., Istituto Nazionale di Geofisica e Vulcanologia, Roma.

708  
709 Demoulin, A., Beckers, A. & Hubert-Ferrari, A. (2015). Patterns of Quaternary uplift of the Corinth rift  
710 southern border (N Peloponnese, Greece) revealed by fluvial landscape morphometry. *Geomorphology*  
711 246, 188–204. doi:10.1016/j.geomorph.2015.05.032.

712  
713 Ferentinos, G., Papatheodorou, G., & Collins, M. (1988). Sediment Transport processes on an active  
714 submarine fault escarpment: Gulf of Corinth, Greece. *Marine Geology*, 83 (1-4), 43-61.

715  
716 Fuchs, M. (2007). An assessment of human versus climatic impacts on Holocene soil erosion in NE  
717 Peloponnese, Greece. *Quaternary Research*, 67 (3), 349-356.

718  
719 Galanopoulos, A., Delimbasis, N., & Comninakis, P. (1964). A tsunami generated by a slide without a  
720 seismic shock. *Geological Chronicles of Greece*, 16, 93-110.

721  
722 Hasiotis, T., Charalampakis, M., Stefatos, a., Papatheodorou, G. & Ferentinos, G. (2006). Fan delta de-  
723 velopment and processes offshore a seasonal river in a seismically active region, NW Gulf of Corinth.  
724 *Geo-Marine Letters*, 26, 199–211. doi:10.1007/s00367-006-0020-8.

725  
726  
727 Heezen, B. C., Ewing, M., & Johnson, G. L. (1966). The Gulf of Corinth floor. *Deep-Sea research*, 13,  
728 381-411.

729  
730 Kontopoulos, N., & Avramidis, P. (2003). A late Holocene record of environmental changes from the  
731 Aliko lagoon, Egion, North Peloponnesus, Greece. *Quaternary International*, 111 (1), 75-90.

732  
733 Koukouvelas, I. K., Katsonopoulou, D., Soter, S., & Xypolias, P. (2005). Slip rates on the Helike Fault,  
734 Gulf of Corinth, Greece: New evidence from geoarchaeology. *Terra Nova*, 17 (2), 158-164.

735  
736 Kortekaas, S., Papadopoulos, G.A., Ganas, A., Cundy, A., & Diakantoni, A. (2011). Geological  
737 identification of historical tsunamis in the Gulf of Corinth, Central Greece. *Natural Hazards and Earth*  
738 *System Science*, 11 (7), 2029-2041.

739 | [Leeder, M. R., Harris, T., & Kirkby, M. J. \(1998\). Sediment supply and climate change: implications for](#)  
740 [basin stratigraphy. Basin Research, 10 , 7-18.](#)  
741  
742  
743 Lorito, S., Tiberti, M. M., Basili, R., Piatanesi, A., & Valensise, G. (2008). Earthquake-generated  
744 tsunamis in the Mediterranean Sea: Scenarios of potential threats to Southern Italy. *Journal of*  
745 *Geophysical Research*, 113 (B1), B01301.  
746  
747 Lykousis, V., Sakellariou, D., Rousakis, G., Alexandri, S., Kaberi, H., Nomikou, P., Georgiou P. &  
748 Balas, D. (2007). Sediment failure processes in active grabens: the western gulf of Corinth (greece). in  
749 V. Lykousis, D. Sakellariou, & J. Locat (Éds.), *Submarine Mass Movements and their Consequences III*  
750 (pp. 297-305). Springer.  
751  
752 Lykousis, V., Roussakis, G., & Sakellariou, D. (2009). Slope failures and stability analysis of shallow  
753 water prodeltas in the active margins of Western Greece, northeastern Mediterranean Se. *International*  
754 *Journal of Earth Sciences*, 98 (4), 807-822.  
755  
756 McNeill, L., Cotterill, C., Henstock, T., Bull, J., Stefatos, A., Collier, R., Papatheoderou, G., Ferentinos,  
757 G., & Hick S.E. (2005). Active faulting within the offshore western Gulf of Corinth, Greece:  
758 Implications for models of continental rift deformation. *Geology*, 33 (4), 241.  
759  
760 Moernaut, J., De Batist, M., Charlet, F., Heirman, K., Chapron, E., Pino, M., Brümmer, R. & Urrutia, R.  
761 (2007). Giant earthquakes in South-Central Chile revealed by Holocene mass-wasting events in Lake  
762 Puyehue. *Sedimentary Geology* 195, 239–256. doi:10.1016/j.sedgeo.2006.08.005.  
763  
764 Moernaut, J., De Batist, M., Heirman, K., Van Daele, M., Pino, M., Brümmer, R., & Urrutia, R. (2009).  
765 Fluidization of buried mass-wasting deposits in lake sediments and its relevance for paleoseismology:  
766 Results from a reflection seismic study of lakes Villarrica and Calafquen (South-Central Chile).  
767 *Sedimentary Geology*, 213 (3-4), 121-135.  
768  
769 Moernaut, J., & De Batist, M. (2011). Frontal emplacement and mobility of sublacustrine landslides:  
770 Results from morphometric and seismostratigraphic analysis. *Marine Geology* 285 (2011) 29–45,  
771 doi:10.1016/j.margeo.2011.05.001  
772  
773 Moernaut, J., Van Daele, M., Strasser, M., & De Batist, M. (2015). A lacustrine perspective on turbidite  
774 and landslide cycles : implications for subaquatic paleoseismology. *Turbidites: process and records*, in:  
775 Oral communication at the ISC 2015, Geneva.  
776  
777 Moretti, I., Lykousis, V., Sakellariou, D., Reynaud, J.-Y., Benziane, B., & Prinzhofer, A. (2004).  
778 Sedimentation and subsidence rate in the Gulf of Corinth: what we learn from the Marion Dufresne's  
779 long-piston coring. *Comptes Rendus Geoscience*, 336 (4-5), 291-299.  
780  
781 Nomikou, P., Alexandri, M., Lykousis, V., Sakellariou, D., & Ballas, D. (2011, September). Swath  
782 bathymetry and morphological slope analysis of the Corinth Gulf. In Grützner C. Pérez-López R.  
783 Fernandez Steeger T. Papanikolaou I. Reicherter K. Silva PG & Vött A.(eds) *Earthquake Geology and*  
784 *Archaeology: Science, Society and Critical Facilities*. 2nd INQUA-IGCP-567 International Workshop  
785 on Active Tectonics, Earthquake Geology, Archeology and Engineering, 19-24.  
786  
787 Pantosti, D., De Martini, P. M., Koukouvelas, I., Stamatopoulos, L., Palyvos, N., Pucci, S., Lemielle, F.,  
788 & Pavlides, S. (2004). Palaeoseismological investigations of the Aigion Fault (Gulf of Corinth, Greece).  
789 *Comptes Rendus Geoscience* , 336 (4-5), 335-342.  
790  
791 Papadopoulos, G. A. (2003). Tsunami Hazard in the Eastern Mediterranean : Strong Earthquakes and  
792 Tsunamis in the Corinth Gulf , Central Greece. *Natural Hazards*, 29, 437-464.  
793

794 Papatheodorou, G., & Ferentinos, G. (1993). Sedimentation processes and basin-filling depositional  
795 architecture in an active asymmetric graben: Strava graben, Gulf of Corinth, Greece. *Basin Research* 5,  
796 235–253. doi:10.1111/j.1365-2117.1993.tb00069.x.

797

798 Papatheodorou, G., & Ferentinos, G. (1997). Submarine and coastal sediment failure triggered by the  
799 1995, M = 6.1 R Aegion earthquake, Gulf of Corinth, Greece. *Marine Geology*, 137, 287-304.

800

801 Papathoma, M., & Dominey-Howes, D. (2003). Tsunami vulnerability assessment and its implications  
802 for coastal hazard analysis and disaster management planning, Gulf of Corinth, Greece. *Natural Hazards*  
803 and *Earth System Science*, 3 (6), 733-747.

804

805 Perissoratis, C., Piper, D. J., & Lykousis, V. (2000). Alternating marine and lacustrine sedimentation  
806 during late Quaternary in the Gulf of Corinth rift basin, central Greece. *Marine geology*, 167, 391-411.

807

808 Salamon, A., Rockwell, T., Ward, S. N., Guidoboni, E., & Comastri, A. (2007). Tsunami Hazard  
809 Evaluation of the Eastern Mediterranean: Historical Analysis and Selected Modeling. *Bulletin of the*  
810 *Seismological Society of America*, 97 (3), 705-724.

811

812 Soloviev, S. L. (1990). Tsunamigenic zones in the Mediterranean Sea. *Natural Hazards*, 3 (2), 183-202.

813

814 Stefatos, A., Charalambakis, M., Papatheodorou, G., & Ferentinos, G. (2006). Tsunamigenic sources in  
815 an active European half-graben (Gulf of Corinth, Central Greece). *Marine Geology*, 232 (1-2), 35-47.

816

817 Strasser, M., Anselmetti, F. S., Fah, D., Giardini, D., & Schnellmann, M. (2006). Magnitudes and source  
818 areas of large prehistoric northern Alpine earthquakes revealed by slope failures in lakes. *Geology*, 34  
819 (12), 1005.

820

821 Strasser, M., Monecke, K., Schnellmann, M., & Anselmetti, F.S. (2013). Lake sediments as natural  
822 seismographs: A compiled record of Late Quaternary earthquakes in Central Switzerland and its  
823 implication for Alpine deformation. *Sedimentology*, 60, 319–341. doi:10.1111/sed.12003.

824

825 [Taylor, B., Weiss, J. R., Goodliffe, A. M., Sachpazi, M., Laigle, M., & Hirn, A. \(2011\). The structures,  
826 stratigraphy and evolution of the Gulf of Corinth rift, Greece. \*Geophysical Journal International\*, 185,  
827 1189-1219.](#)

828

829 Tinti, S., Zaniboni, F., Armigliato, A., Pagnoni, G., Gallazzi, S., Manucci, A., Brizuela Reyes B.,  
830 Bressan L., & Tonini, R., (2007). Tsunamigenic landslides in the western Corinth Gulf: numerical  
831 scenarios. In V. Lykousis, & D. Sakellariou (Éds.), *Submarine Mass Movements and their*  
832 *Consequences* (pp. 405-414). Springer.

833

834 Tripsanas, E. K. & Piper, D.J.W. (2008). Glaciogenic Debris-Flow Deposits of Orphan Basin, Offshore  
835 Eastern Canada: Sedimentological and Rheological Properties, Origin, and Relationship to Meltwater  
836 Discharge. *Journal of Sedimentary Research*, 78, 724-744.

837

838 Urlaub, M., Talling, P.J., & Masson, D.G. (2013). Timing and frequency of large submarine landslides:  
839 Implications for understanding triggers and future geohazard. *Quaternary Science Reviews*, 72, 63–82.  
840 URL: Link, doi:10.1016/j.quascirev.2013.04.020.

841

842 Van Welden, A. (2007). Enregistrements sédimentaires imbriqués d'une activité sismique et de  
843 changements paléo-environnementaux. Etude comparée de différents sites: Golfe de Corinthe (Grèce),  
844 Lac de Shkodra (Albanie/Montenegro), Golfe de Cariaco (Vénézuéla). PhD thesis, University of  
845 Savoie

846

847 Woessner, J., Giardini, D., & Danciu, L. (2013). SHARE project, D5. "Final seismic hazard assessment  
848 including aggregation. Tech. rep., Swiss Seismological Service.

849

850 Zitter, T.A.C., Grall, C., Henry, P., Ozeren, M.S., Cagatay, M.N., Sengor, A.M.C., Gasperini, L., de  
851 Lépinay, B.M., & Géli, L. (2012). Distribution, morphology and triggers of submarine mass wasting in  
852 the Sea of Marmara. *Marine Geology* 329-331, 58–74. doi:10.1016/j.margeo.2012.09.002.